LIMNOLOGY
and
OCEANOGRAPHY

ASLO

Limnol. Oceanogr. 60, 2015, 1371–1381

doi: 10.1002/lno.10104

Observations of tidal and storm surge attenuation in a large tidal marsh

J. Stark,*[1] T. Van Oyen,[2,3] P. Meire,[1] S. Temmerman[1]

[1]Ecosystem management research group, Department of Biology, University of Antwerp, Wilrijk, Belgium
[2]Flanders Hydraulics Research, Antwerp, Belgium
[3]Department of Civil Engineering, Ghent University, Zwijnaarde, Belgium

Abstract

Tidal wetlands are increasingly valued for their role in coastal defense. Nevertheless, in situ observations of storm surge attenuation within wetlands are still scarce. We present water level measurements along a 4 km intertidal channel and on the surrounding marsh platform for regular spring to neap tides and two major storm surge tides, showing the effects of flood wave height and marsh geomorphology on the amount of flood wave attenuation. Undermarsh tides with peak water levels below marsh platform elevation are mostly amplified (up to 4 cm/km) within the channels. Overmarsh tides with peak water levels above the marsh platform are generally attenuated along the channels, with maximum attenuation rates of 5 cm/km for tides that inundate the marsh platform by 0.5–1.0 m. For lower or higher flood waves, including storm surges, attenuation rates decrease. Furthermore, the observations show that the maximum attenuation occurs along narrow channel transects where the width of the platform is larger, whereas attenuation rates are lower along wider channels with smaller adjacent marsh platforms. These observations are confirmed by an analytical approximation of tidal wave propagation through convergent channels. The analytical model indicates that differences in attenuation rates are induced by variations in the cross-channel averaged friction between channel sections and between tides with varying peak water levels. Finally, the highest attenuation rates of up to 70 cm/km are observed over short distances on the vegetated marsh platform. We conclude that this study provides an empirical basis for the wider implementation of nature-based flood defense strategies.

Low-lying coastal areas are vulnerable to flood hazards caused by storm surges. Global change is expected to increase the risks of flood disasters due to accelerating sea level rise, increasing storm intensity, and growing coastal populations (e.g., Nicholls and Cazenave 2010; Woodruff et al. 2013). As a consequence there is a worldwide growing need for long-term sustainable adaptation to storm surge flood risks, in particular for low-lying deltas and estuaries. Tidal wetlands, including salt marshes and mangroves, are increasingly recognized for their potential value as natural protective barriers (Wamsley et al. 2009; Temmerman et al. 2013). They can reduce the height of wind waves (Möller et al. 2014) and storm surges through additional vegetation roughness and thereby reduce the associated damage during extreme flood events (Costanza et al. 2008; Shepard et al. 2011; Barbier et al. 2013). Tidal wetlands are nowadays starting to be implemented as naturally sustainable coastal defense systems (Temmerman et al. 2013), which calls for a better understanding of flood level reduction by marshes.

*Correspondence: jeroen.stark@uantwerpen.be

In situ observations of peak water level reduction in coastal wetlands are scarce. Most of the existing field studies considered storm surge attenuation for only one or a few specific hurricane-induced surge events and reported a wide range of attenuation rates, from about 4 cm to 25 cm of peak water level reduction per kilometer of wetland (Lovelace 1994; McGee et al. 2006; Krauss et al. 2009; Wamsley et al. 2010). An overview of attenuation rates in coastal marshes and mangroves found in previous field studies is shown in Table 1. The large variety in observed storm surge attenuation rates suggests that the attenuation capacity largely depends on the properties of the specific wetland location and specific storm event. Numerical modeling studies have indeed shown that storm surge reduction within coastal marshes varies with site-specific variables, such as offshore bathymetry (Resio and Westerink 2008), marsh geomorphology, including marsh vegetation cover and local surface roughness (e.g., Loder et al. 2009; Temmerman et al. 2012; Zhang et al. 2012), and with the presence of man-made levees (e.g., Wamsley et al. 2010). These studies have also shown that storm surge reduction may vary with

Table 1. Observed attenuation rates in wetlands from previous field studies

Location	Description	Attenuation rate (cm/km)	Reference
Louisiana	Hurricane Andrew (1992) surge reduction over 37 km of marsh and open water	4.4–4.9	Lovelace (1994), Wamsley et al. (2010)
Great Marshes, Massachusetts	Mean HWL variation across tidal flats and salt marsh channels	−2.0*−11.0	Calculated from figures in Van der Molen (1997)
Ten Thousand Islands National Wildlife Refuge, Florida	Hurricane Charley (2004) surge reduction across 5.5 km of marshes and mangroves	9.4–15.8	Krauss et al. (2009)
Shark River (Everglades), Florida	Hurricane Wilma (2005) surge reduction over 14 km of riverine mangrove	4.0–6.9	Krauss et al. (2009)
Cameron Prairie, Louisiana	Hurricane Rita (2005) surge reduction in marsh area	10.0	McGee et al. (2006), Wamsley et al. (2010)
Sabine, Louisiana	Hurricane Rita (2005) surge reduction in marsh area	25.0	McGee et al. (2006), Wamsley et al. (2010)
Vermillion, Louisiana	Hurricane Rita (2005) surge reduction in marsh area	4.0	McGee et al. (2006), Wamsley et al. (2010)
Vermillion, Louisiana	Hurricane Rita (2005) surge reduction in marsh area	7.7	McGee et al. (2006), Wamsley et al. (2010)

*Negative values denote that amplification was observed.

event-specific variables, such as storm surge height, storm track and duration (e.g., Resio and Westerink 2008; Loder et al. 2009; Wamsley et al. 2010). Moreover, modeling studies indicate that larger surge events with higher marsh platform inundation depths are less effectively attenuated than smaller surge events with lower marsh inundation depths and shorter durations (Loder et al. 2009). However, systematic field data of events with varying marsh inundation depths, ranging from low tidal inundations to extreme storm surges, are lacking. Even field studies on the attenuation of regular tides in marshes are very scarce. To our knowledge, the only available field study on attenuation of regular tides in a large tidal marsh was conducted by Van der Molen (1997), who focused mainly on spatial differences in mean high water level (HWL) in a tidal marsh along the U.S. Atlantic coast, showing a reduction of mean HWLs of up to 11 cm/km. Field studies that assess the impact of different marsh inundation depths on tidal and storm surge propagation through marshes are to our knowledge not yet available.

Here, we present a coherent set of field observations on peak water level variations within a large tidal marsh, covering a wide range of marsh inundation depths including neap to spring tides and two storm surges. These observations lead to new insights which are discussed in the Discussion section. In addition, in the Discussion section, we demonstrate that our findings are consistent with the results of a simplified one-dimensional (1D) analytical model for tidal wave propagation in converging channels which is based on the wave energy flux balance (Van Rijn 2011). Finally, as large scale in situ water level observations in tidal marshes are scarce, the data presented in this study provides a valuable dataset to validate numerical modeling studies describing the propagation of tidal waves and storm surges in coastal wetlands.

Methods

Field measurements were conducted in the Saeftinghe marsh, a more than 3000 ha brackish tidal marsh along the Western Scheldt estuary (SW Netherlands; 51.3671 °N, 4.1760 °E). The local tidal regime is semidiurnal with HWLs varying between 2.18 m and 3.15 m NAP (NAP is the Dutch ordnance level, close to mean sea level) and a tidal range between 4.02 m and 5.57 m for neap and spring tides respectively. Approximately 70% of Saeftinghe is occupied with marsh vegetation. The marsh vegetation is dominated by *Elymus athericus* and *Scirpus maritimus*, while other species occur in lower densities, including *Puccinellia maritima, Aster tripolium* and patches of *Phragmites australis*. The mean canopy height of *E. athericus*, the most abundant species in our study area, is 0.43 m with a standard deviation of 0.1 m (Vandenbruwaene et al. 2015). The remaining 30% of the marsh consists of bare tidal flats and an extensive intertidal channel system (i.e., channels which are dry during low tides).

Water level measurements were done in and along the 4 km long Hondegat channel which is over 500 m wide near the main estuarine channel and branches in the landward direction into an extensive network of smaller creeks (Fig. 1). The marsh platform elevation surrounding this channel varies between 2.89 m and 3.45 m NAP, calculated as the 10% and 90% percentiles from a Lidar based digital elevation

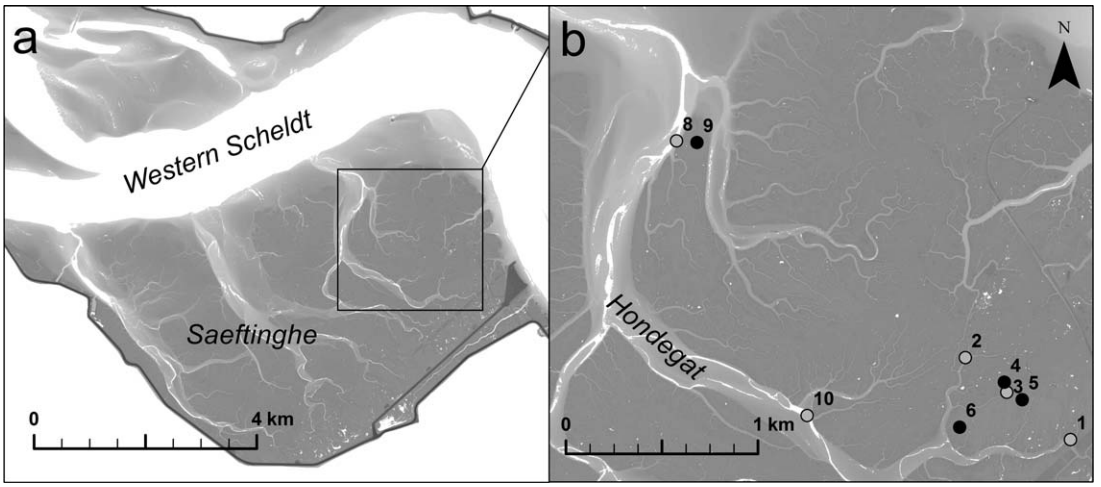

Fig. 1. Study area in the Western Scheldt estuary: (a) Saeftinghe marsh and (b) the Hondegat channel with locations of water level measurements in the marsh channels (light dots) and on the marsh platform (dark dots).

model. Water levels were measured during two periods of approximately 1 month (28 August 2013–06 October 2013 and 05 December 2013–31 December 2013) at several locations in the channel and on the marsh platform. Figure 2 shows typical observations at the various locations (*see* Fig. 1) of the water level variation for different conditions; i.e., for undermarsh tides (Fig. 2a), overmarsh tides (Fig. 2b) and storm tide (Fig. 2c). The second measurement series includes a severe storm surge that coincided with spring tide and caused two storm tides. The highest storm tide induced peak water levels at several tidal stations in the Western Scheldt estuary which correspond to a 1/8 - 1/20 yr^{-1} exceedance probability (water level exceedance probabilities for tidal stations are obtained from Rijkswaterstaat, http://www.rijkswaterstaat.nl). In particular, HWLs at the estuary mouth and at tidal stations near the study area were approximately 1.50 m above the astronomical tide during the highest storm tide. While the storm surge was forced by strong northwestern winds on the North Sea, local wind conditions in the study area were less strong at the time HWLs arrived at the entrance of the marsh. In particular, observations from weather stations near the study area indicated hourly averaged wind speeds of 8–11 m/s from a west- to northwest direction during the storm tide's high water slack, while maximum wind speeds of 21–24 m/s were measured in the Dutch part of the North Sea (wind data obtained from Royal Netherlands Meteorological Institute, http://www.knmi.nl). Local wind conditions were milder because the study area is located approximately 60 km inland from the estuary mouth in the North Sea and wind speeds were generally lower there. Second, the peak water levels only reached the study area several hours after the peak of the storm.

The configuration of the measurement locations during the first measurement period consists of one location in the main channel at the marsh edge (location 8), one location in the main channel at the backside of the marsh (location 1), two locations in smaller side-channels at the backside of the marsh (locations 2 and 3) and four locations on the marsh platform (locations 4–6 and 9). During the second campaign measurement devices were only deployed at locations 1, 3, 5, and 8, while location 10 was added halfway the main channel between locations 1 and 8. Locations 1–3 are all situated at approximately similar distances from the marsh edge, measured along the channel system. However, the channels toward these locations vary in width, depth and cross-sectional area (Table 2). Location 1 is situated in the relatively wide main channel, whereas locations 2 and 3 are situated in narrower side-channels with smaller cross-sectional areas. In general, there is a gradual convergence in channel width from $\sim$ 500 m to $\sim$ 30 m between locations 8, 10, and 1, whereas the decrease in channel width toward location 2 and especially location 3 is more abrupt at the entrance of the side-channels. The configuration of measurement locations allows for a comparison of the tidal wave at the marsh edge (location 8) with tides and peak water levels at a variety of sites that are located approximately 4 km from the marsh edge, providing insight into the propagation and attenuation of tides and storm surges in the marsh.

Water level loggers (Schlumberger, Mini-divers and CERA-divers) were used for the field observations. This equipment contains a pressure sensor that measures the water surface level with an accuracy of $\pm$ 1 cm. A BARO-diver, which records the atmospheric pressure, was installed nearby the study area to compensate the water level measurements for the atmospheric pressure (accuracy $\pm$ 0.5 cm). The measurement frequency was set to 2 min to record the flood propagation accurately. Horizontal coordinates and vertical elevations of the measurement points were determined with

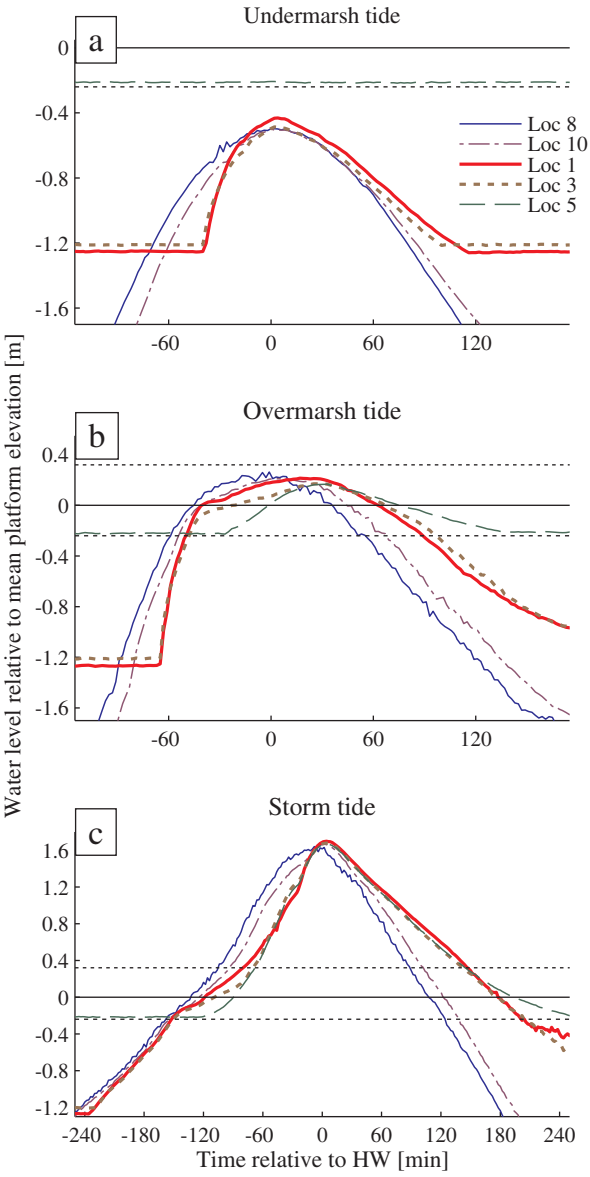

Fig. 2. Tidal water levels at several marsh locations in the channel network (locations 1, 3, 8, and 10) and on the marsh platform (location 5) for: (a) a typical undermarsh tide (10 December 2013), (b) a typical overmarsh tide (05 December 2013) and (c) the highest recorded storm tide (06 December 2013). The overall mean marsh platform elevation is indicated with a solid horizontal line, and 10% and 90% percentiles with dashed horizontal lines. [Color figure can be viewed in the online issue, which is available at wileyonlinelibrary.com.]

RTK-GPS (Trimble 5800), obtaining a vertical precision of ± 1 cm and ± 2 cm for the first and second campaign respectively.

Results

To evaluate the attenuation rate along the intertidal channels within the marsh, we assess the flood attenuation rate between the marsh edge (location 8) and the inner marsh locations (locations 1–3) in Fig. 3a, while Fig. 3b shows the difference in peak water level between location 10 and locations 1–3. Attenuation rates are calculated as the reduction in peak water level between two locations in cm/km. The figures show that the attenuation rate can vary significantly between individual flood events depending on the height of the peak water level. For overmarsh tides (i.e., peak water level above mean platform elevation), the overall attenuation rate from the marsh edge to the inner marsh locations (Fig. 3a) increases for higher HWL and reaches a maximum of 4–5 cm/km for flood events with peak water levels of 0.5–1.0 m above the mean marsh platform elevation. The attenuation rate decreases again for higher tides and there is even a slight amplification measured for the highest recorded storm tide. Conversely, it is observed that when undermarsh tides occur (i.e., considering HWL below mean platform elevation) the flood attenuation strongly decreases or changes to amplification.

Second, Fig. 3 shows that the attenuation rate also varies between different channels in the inner marsh area. In particular, attenuation rates measured along transects through the relatively wide main channel (toward location 1, *see* Table 1) are generally lower than those in the narrower side-channels (toward locations 2–3). For example, considering undermarsh tides, this results in an amplification of the peak water level within the main channel of the marsh (up to 4 cm/km between location 10 and location 1; Fig. 3b); while in the side-channels, there is still a small decrease of the peak water level (location 2) or the amplification is not so pronounced (location 3). Moreover, the attenuation rates and the amplification rates measured along the wide outer marsh transect (location 8–10) are lower than those measured along the narrower inner marsh transects (location 10–1 and 3). Finally, the maximum measured flood wave attenuation over the whole length of the channel system is about 15 cm (or 4 cm/km) from the marsh edge (location 8) toward locations 2 and 3. The maximum attenuation rate within parts of the channel system is approximately 5 cm/km from location 10 toward locations 1 and 3. The maximum attenuation between location 10 and location 2 is not calculated as there are no simultaneous measurements at these locations.

Over non-channeled transects on the vegetated marsh platform, in general, it is found that the peak water level is attenuated, regardless the HWL (*see* Fig. 4). Calculated attenuation rates based on the field measurements can rise up to 70 cm/km (Fig. 4) which is an order of magnitude higher than the maximum rates calculated over transects through the channels (up to 5 cm/km; Fig. 3b). It must however be stated that the attenuation rates over the marsh platform have been measured over relatively short distances (50–100 m), meaning that the total measured attenuation over these short transects on the platform was only up to 7 cm.

Figure 5 illustrates the changes in the vertical tidal asymmetry as the tide propagates through the marsh. At the

Table 2. Geometrical properties of channel cross-sections at the measurement locations in the marsh channel system, showing channel width (w), mean channel depth below MHWL (h_{mean}), maximum channel depth below MHWL (h_{max}) and cross-sectional area (A_c)

Location		Lat. (°)	Lon. (°)	w (m)	h_{mean} (m)	h_{max} (m)	A_c (m^2)
8	Marsh edge	51.3695	4.1795	517	2.1	3.9	1105
10	Main channel	51.3565	4.1897	167	1.2	2.2	206
1	Main channel	51.3559	4.2092	30	0.4	1.1	12
2	Side-channel	51.3596	4.2012	8	0.8	1.1	6
3	Side-channel	51.3581	4.2044	4	0.5	0.7	2

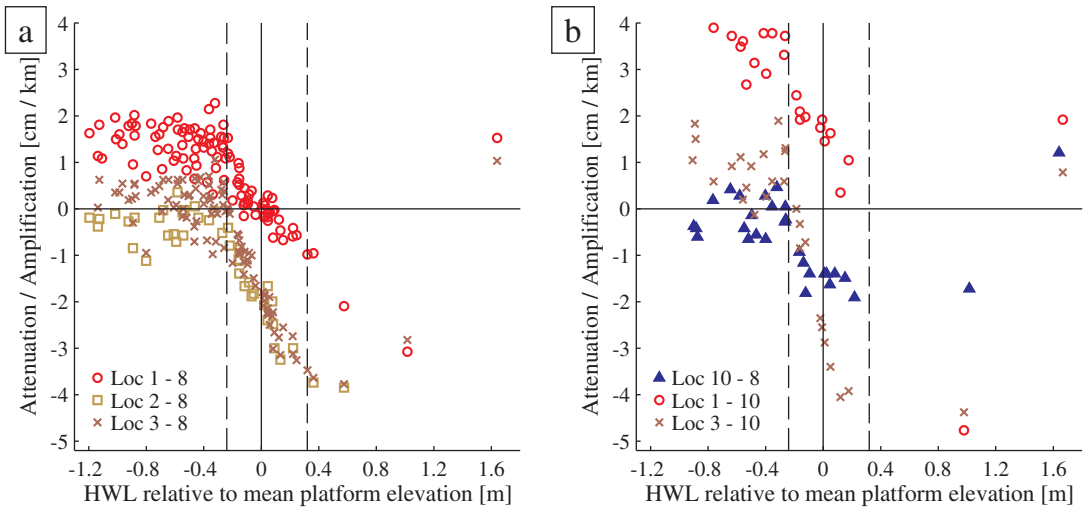

Fig. 3. Amplification and attenuation rates (a) between several inner marsh locations and the marsh edge, and (b) over shorter transects within the marsh channel network (*see* Fig. 1 for locations). Amplification and attenuation rates are calculated as the vertical difference in peak water levels in cm per km between locations. The overall mean marsh platform elevation is indicated with a solid vertical line, and 10% and 90% percentiles with dashed vertical lines. [Color figure can be viewed in the online issue, which is available at wileyonlinelibrary.com.]

marsh edge (location 8, symbols in blue in Fig. 5a), the ratio R between flooding period T_{flood} and ebb period T_{ebb} is found to vary between 0.7 and 1.2; i.e., both flood-dominant and ebb-dominant asymmetry is observed at the marsh edge. Figure 5b describes the ratio between R at location 1 and R at location 8 to quantify the changes in the vertical asymmetry along the main channel. It is found that R decreases from the marsh edge (location 8) toward the inner marsh (location 1, symbols in red in Fig. 5a) for almost all tides. Hence, the tidal asymmetry becomes more flood-dominant (i.e., shorter flood period than ebb period) from the marsh edge toward the end of the main channel. Moreover, the flood-dominant asymmetry at the inner marsh location gets stronger with increasing peak water levels as long as the marsh platform does not get inundated. As illustrated by Fig. 5a, at the transition from undermarsh to overmarsh tides, tidal asymmetry at the inner marsh location 1 changes abruptly toward a less flood-dominant ratio. Conversely, there is no measurable effect of platform inundation at the marsh edge location 8. As a result, the difference in tidal asymmetry between the marsh edge and inner marsh location becomes smaller again. This abrupt change in tidal asymmetry at location 1 can also be observed directly from the water level recordings of overmarsh tides as depicted in Fig. 2, which show that water levels rise slower at inner marsh locations from the moment the platform becomes inundated. As peak water levels increase further above the platform elevation, flood-dominance at the inner marsh location 1 becomes stronger again. Finally, the highest recorded storm tides result in the lowest ratio between flood and ebb periods at location 1 (Fig. 5). This in contrast to location 8, where the two storm tides were even ebb-dominant due to elongated flood periods of over 6 h, compared to around 3–4 h during normal tides at this location.

Discussion

While direct measurements of attenuation of tides and storm surges in tidal wetlands (e.g., Van der Molen 1997; Krauss et al. 2009) are scarce and present insights on storm

surge attenuation in wetlands are largely based on numerical modeling (e.g., Loder et al. 2009; Wamsley et al. 2010; Temmerman et al. 2012), we performed in situ measurements of tidal propagation within a large tidal wetland for a wide range of flood events, ranging from neap to spring tides and including two storm surge events. The results of our field study show that the amount of peak water level attenuation along the marsh channels varies with the inundation height above the marsh platform elevation and with the width of channels (relative to the platform width) that dissect the marsh platform (Table 2). The measured attenuation rates for tidal peak water levels in the marsh channel system are in the range of attenuation rates found in previous studies on hurricane-induced surges propagating through mangroves and coastal wetlands (Lovelace 1994; Krauss et al. 2009; Wamsley et al. 2010) and of attenuation rates calculated from observed spatial differences in mean HWLs in a large tidal marsh by Van der Molen (1997) (Table 1).

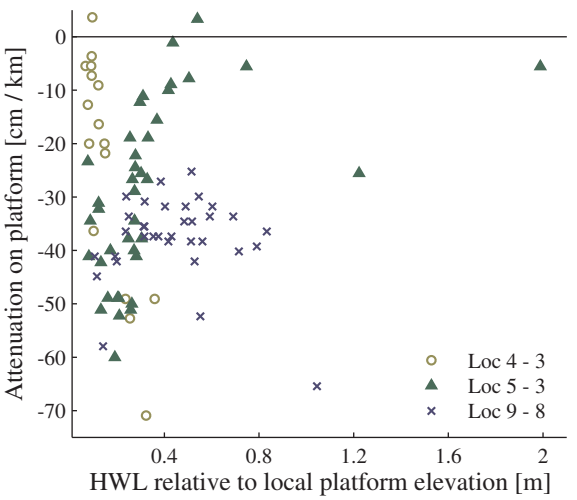

Fig. 4. Attenuation rates between locations on the marsh platform and nearby locations in a marsh channel (*see* Fig. 1 for locations), calculated as the vertical difference in peak water levels in cm per km in between locations. [Color figure can be viewed in the online issue, which is available at wileyonlinelibrary.com.]

Comparison with analytical models for tidal flow in tidal channels

The propagation of overmarsh tides in our observations, which is influenced by both channel geometry and marsh platform characteristics, shows similarities with the characteristics of propagating tides in convergent tidal basins with large intertidal storage area, based on approximate analytical models. In addition, the observed propagation of undermarsh tides, which is mainly influenced by channel geometry, shows similarities with propagating tides in convergent tidal basins with little intertidal storage. For instance, Friedrichs and Aubrey (1994) and Van Rijn (2011) illustrate analytically that tidal wave propagation in convergent channels is dominated by a balance between friction effects (causing attenuation) and convergence (causing amplification). In our observations the amplified undermarsh tides appear to be dominated by convergence, while for the attenuated overmarsh tides friction dominates over convergence. Similarly, Friedrichs and Madsen (1992) found that shallow embayments with large tidal amplitude to water depth ratios and relatively little intertidal storage induce a water level set up and a (flood-dominant) shorter rising asymmetry, whereas shallow embayments with ample intertidal storage and low amplitude to depth ratios induce a set down and an (ebb-dominant) shorter falling asymmetry. In our observations,

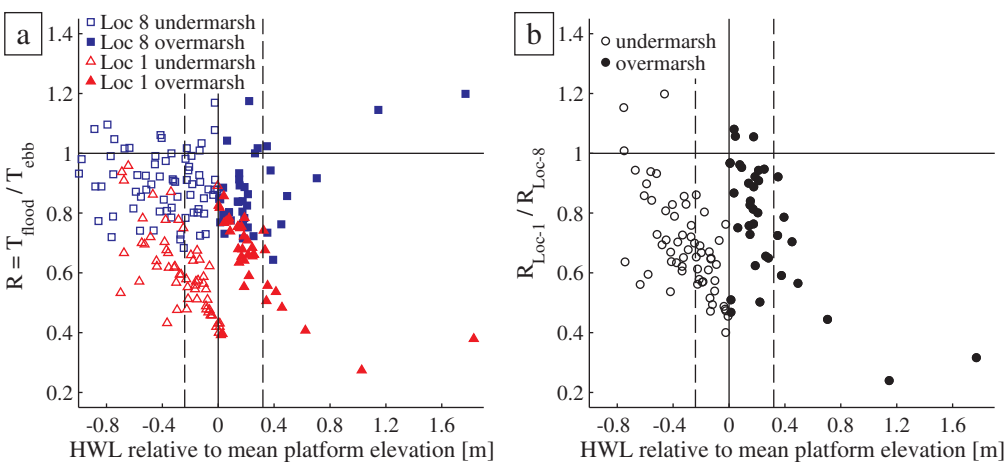

Fig. 5. (a) Tidal asymmetry, expressed as the ratio *R* between the duration of the flood and ebb period, at the marsh edge (location 8, blue squares) and the inner marsh (location 1, red triangles) for different undermarsh tides (open symbols) and overmarsh tides (filled symbols), with the global mean platform elevation (solid vertical line) and the 10% and 90% percentiles (dashed vertical lines). (b) Relative change in tidal asymmetry from the outer marsh location toward this inner marsh location. Flood and ebb periods were calculated for the period that water levels were above the water level loggers (i.e., −0.4 m NAP at location 8 and 2.1 m NAP at location 1). [Color figure can be viewed in the online issue, which is available at wileyonlinelibrary.com.]

undermarsh tides show an increase in shorter rising asymmetry from the marsh edge toward the end of the main channel and this increase in flood-dominant asymmetry does indeed get smaller at the moment the platform gets inundated (Fig. 5). The ebb-dominant shorter falling asymmetry as described by Friedrichs and Madsen (1992), however, does not occur at the inner marsh locations.

To investigate whether the insights following from the presented observations are generic and not only site-specific, we use the analytical model of Van Rijn (2011) which is based on a basic consideration of the conservation of wave energy flux. It should however be stated that it is not the intention to fit this 1D analytical model to the observed data, as the application of the model to the presented results is not straightforward. In particular, the model is conceived for an idealized setting and is built upon several approximations which are not completely valid for the present situation; e.g., the representation of the tidal wave as a single progressive sinusoidal wave is a rather crude approximation (Van Rijn 2011), the complex marsh geometry is simplified to a 1D schematization and the model does not account for wetting and drying processes which occur when the channels are dry. Instead, we use the analytical solution of Van Rijn (2011) solely to investigate the generic character of our findings and to indicate the physical mechanisms that cause the differences in attenuation and amplification rates observed in our measurements. Based on the wave energy flux, Van Rijn (2011) derived that the along-channel variation of the tidal range is governed by the following relation:

$$\frac{dH}{dx} = 0.5\beta\ H(x) - \frac{f\ c^2\ \cos\varphi}{12\pi\ g\ h^3} H(x)^2 \tag{1}$$

in which we have made the additional assumption that the channel depth is constant. In (1), $H(x)$ is the tidal range at distance x from the estuary mouth (or marsh edge in our case), β represents the width convergence coefficient, and h the constant mean water depth. Frictional effects on the tidal wave propagation are represented by f, a friction coefficient, which is evaluated as $f = 8\ g/C^2$ with C the Chézy coefficient. Finally, g is the gravitational acceleration, $c = (gh)^{0.5}$ the local wave speed and φ the phase lead of velocity maximum with respect to water level maximum. As boundary condition, we consider that at the marsh boundary H is equal to H_0. Equation 1 can then be solved analytically, yielding:

$$H(x) = \left(\left(\frac{C_a + C_b\ H_0}{H_0\ C_a} \right) e^{(-C_a\ x)} - \frac{C_b}{C_a} \right)^{-1} \tag{2}$$

in which C_a and C_b are along-channel constants representing:

$$C_a = 0.5\beta \tag{3}$$

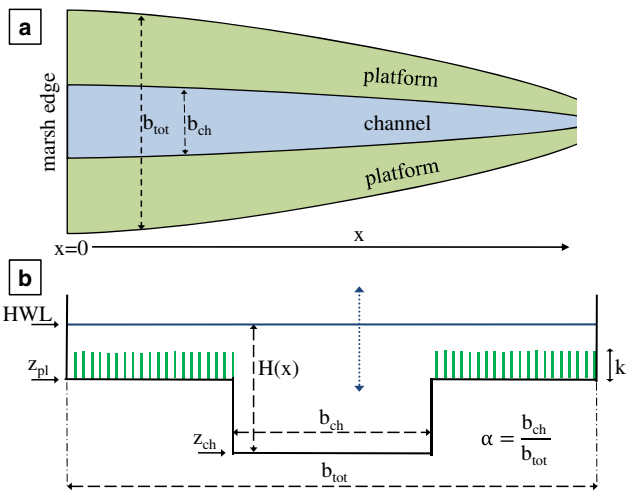

Fig. 6. Schematization of the idealized intertidal channel and adjacent marsh platform, showing (a) a top view of the converging basin and (b) a cross-sectional view of the marsh channel and adjacent platform, in which $H(x)$ is the tidal range, HWL the peak water level, b_{ch} and b_{tot} are the channel and total width respectively, z_{pl} is the elevation of the marsh platform, z_{ch} the elevation of the channel bottom and k the vegetation height. [Color figure can be viewed in the online issue, which is available at wileyonlinelibrary.com.]

$$C_b = -\frac{f\ c^2\ \cos\varphi}{12\pi\ g\ h^3} \tag{4}$$

To take into account the effect of intertidal flats adjacent to the main channel, Van Rijn (2011) further states that h can be replaced by the effective water depth $h_{eff} = (b_{ch}/b_{tot})h_{ch} = \alpha h_{ch}$, with b_{ch} and b_{tot} representing the channel width and total width, respectively. Hence, the scaling factor α can be used to schematize the influence of the marsh platform surrounding the marsh channel.

To apply the analytical solution to an intertidal channel, it is necessary to make some assumptions with respect to the schematization of the marsh (*see* also Fig. 6 for a graphical representation). The tidal range is schematized as the difference between the peak water level at the marsh edge (HWL) and the channel elevation z_{ch}, as the marsh channels fall largely dry during low tide. The tide-averaged water depth in the channel h is assumed to be half of this tidal range and h_{eff} is only used for overmarsh tides (HWL $> z_{pl}$, in which z_{pl} denotes the platform elevation). The Chézy friction coefficient deployed to evaluate Eq. 2 is computed as the width-averaged Chézy coefficient, which means for overmarsh tides that:

$$C = \alpha \times C_{ch} + (1-\alpha) \times C_{pl} \tag{5}$$

with C_{ch} and C_{pl} being the Chézy coefficients representative for the marsh channel and platform, respectively. To implement the effect of vegetation submergence during the highest tides (HWL $> z_{pl} + k$), the friction formula proposed by Baptist et al. (2007) for submerged vegetation is used:

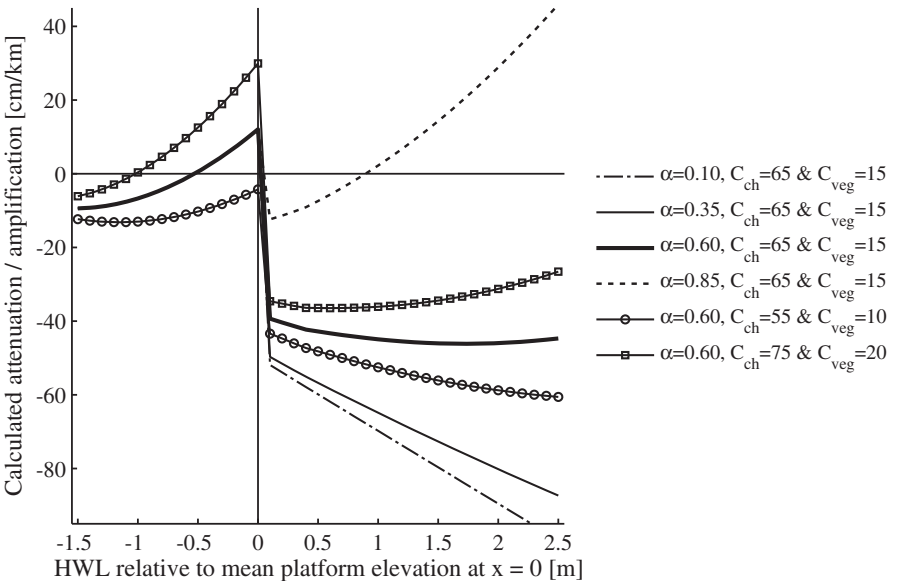

Fig. 7. Results of the analytical model for different Chézy coefficients and different values of α (i.e., ratio between channel width and total width), showing attenuation and amplification rates for varying undermarsh (HWL $< z_{pl}$) and overmarsh (HWL $> z_{pl}$) high water levels at the marsh edge.

$$C_{pl} = C_{veg} + 2 \times \sqrt{g} \times \ln\left(\frac{\mathrm{HWL} - z_{pl}}{k}\right) \quad (6)$$

where C_{veg} is the Chézy coefficient for friction exerted by the vegetation only and k the vegetation height. In case of non-submerged vegetation (HWL $< z_{pl} + k$), C_{pl} equals C_{veg}. Furthermore, we assume all parameters except for $H(x)$ to be constant along the channel axis in x-direction.

The following data have been used to apply the analytical solution to an intertidal channel with adjacent marsh platform. The width convergence length scale $L_b = 1/\beta$ is set equal to 1000 m based on the observed decrease in channel width from the marsh edge location toward the inner marsh locations. The channel elevation $z_{ch} = +0.5$ m is obtained by averaging the elevation of the channel bottom over the full length of the main channel. The platform elevation is set at $z_{pl} = +3.0$ m, close to the mean platform elevation in our study area. The vegetation height is set at $k = 0.4$ m, based on the mean canopy height of the most abundant vegetation type in the study area; i.e., 0.43 m (Vandenbruwaene et al. 2015). To estimate φ, velocity and water level measurements in the main channel close to the marsh edge are used (data obtained from Rijkswaterstaat Zeeland—Meetadviesdienst), leading to $\varphi = 2$ h ($\sim 60°$). Finally, we evaluate the spatial variation of the tidal range for different Chézy friction coefficients as it is not straightforward to derive this parameter from the data; i.e., C_{ch} equal to 55, 65, and 75 $m^{0.5}s^{-1}$ and $C_{veg} = 10$, 15, and 20 $m^{0.5}s^{-1}$. The influence of the marsh platform width on the propagation of overmarsh tides is evaluated by using different values of α (0.1, 0.35, 0.6, and 0.85). Figure 7 shows the resulting amplification and attenuation rates from $x = 0$ m to $x = 5000$ m for varying high water levels (HWL = 1.5–5.5 m) at $x = 0$ m and for the different input values for C and α. The results of the analytical model show that based on a basic consideration of the wave energy flux balance a similar effect of platform inundation is observed as in our observations. Undermarsh tides are increasingly amplified for higher peak water levels; while when the platform gets inundated and h_{eff} and C decrease, friction becomes dominant and attenuation is observed. Depending on the values of C and α, attenuation rates get lower or higher for increasing peak water levels and platform inundation heights. The results show clearly that the width of the platform with respect to the channel width is a key factor to determine whether friction becomes dominant over convergence and tides are attenuated along marsh transects. For higher α values, the computed attenuation rate decreases or turns into amplification for higher peak water levels, whereas attenuation is persistent for increasing peak water levels if α is lower. Hence, the geometrical properties of the marsh channel and platform itself may cause attenuation rates to decrease for increasing inundation heights. Conversely, the Chézy friction coefficients themselves appear to play a minor role in the analytical model. In reality, the extent of the marsh platform that is flooded increases for increasing peak water levels, especially for peak water levels around mean platform elevation (i.e., α varies with varying HWL). This implies that maximum attenuation would occur when the combination of average platform inundation depth, the depth-dependent platform extent and additional

friction exerted by the vegetation induces a maximum cross-sectional averaged friction. All in all, the presented results based upon analytical models for tidal flow in regular tidal basins and estuaries (i.e., channels that are not dry during low tide) support the generic character of our field observations of attenuation and amplification rates in an intertidal channel system.

Effect of inundation height

Our observations indicate that attenuation rates of overmarsh tides first increase for higher platform inundation heights, showing the strongest attenuation for peak water levels that are 0.5–1.0 m above mean platform elevation. Conversely, the highest recorded storm tides were less effectively attenuated or not attenuated at all (Fig. 3). The latter could be a result of the long duration of the flood period of over 6 h during the highest observed storm tide compared to 3–4 h normally. Because of this longer flood duration, more time was available for the storage area on the marsh platform to fill up to similar water levels as in the adjacent estuary. Numerical modeling studies have also shown that surge attenuation along marsh transects decreases for larger surge events if the surge duration is long compared to the time it takes for the storage area on the marsh platform to get fully inundated (Resio and Westerink 2008; Loder et al. 2009; Wamsley et al. 2010). In particular, Resio and Westerink (2008) state that additional friction exerted by a marsh may slow storm surge propagation, but if the hydrodynamic (or wind) forcing is long enough the water will eventually fill up the entire marsh storage area. An additional reason for the decrease in attenuation rates concerns the decreasing flow resistance on the vegetated platform for higher water levels which increasingly submerge the marsh vegetation (Baptist et al. 2007; Nepf 2012). Previous field studies and hydrodynamic modeling studies of regular tides in marshes demonstrated that when the water level is below the vegetation canopy, spatial flow patterns are controlled by friction by the vegetation canopy, while as soon as the water level overtops the vegetation canopy, more large-scale sheet flow over the vegetation canopy can occur (Temmerman et al. 2005a,2005b). Our observations of attenuation rates over the full marsh transect (Fig. 3a) indeed reach a maximum just above the mean canopy height of the most abundant species [i.e., 0.43 m above mean platform elevation; Vandenbruwaene et al. (2014)]. Nevertheless, limitations in storage area on the marsh platform during long inundation events and the decreasing influence of bottom friction for higher inundation events in general can also reduce attenuation rates for higher inundation events.

Effect of channel geometry

The observed attenuation rates vary between different locations in the marsh (Fig. 3), depending on the presence and geometry of nearby channels (Table 2). The measured attenuation rates of overmarsh tides are lowest (up to a maximum of 2 cm/km) along the wide and relatively deep outer marsh transect between locations 8 and 10, where the channel width converges from approximately 520 m to 170 m and where the influence of the marsh platform is relatively small. In terms of the analytical model presented above, values for $\alpha = b_{ch}/b_{tot}$ averaged along the outer marsh transect are estimated to be in the range of 0.4 halfway the main channel to nearly 1.0 at the marsh edge, based on the marsh geometry between the measurement locations. Similarly to the field observations, the results of the analytical model (Fig. 7) show that attenuation of overmarsh tides is smaller for larger values of α. Attenuation rates are higher along the inner marsh transects from location 10 toward location 1 and 3 (up to 5 cm/km), where the channel width decreases further to $\sim$ 4–30 m and the influence of the marsh platform on the propagation of overmarsh tides becomes increasingly important. Averaged values for $\alpha = b_{ch}/b_{tot}$ along the inner marsh transect are estimated to be in the range of 0.1–0.3. Again, the observation of higher attenuation rates for lower values of α is supported by the results of the analytical model (*see* Fig. 7) supporting the generic character of the observations. Furthermore, attenuation rates are generally higher along narrower side-channels toward locations 2 and 3, where the channel width converges to $\sim$ 4–8 m and cross-sectional areas are small, than along the wider main channel toward location 1, where the channel width converges to $\sim$ 30 m and the cross-sectional area is larger. Only for most strongly damped tide, attenuation rates were similar along the inner marsh channels toward locations 1 and 3 (i.e., 5 cm/km). In addition, the observations also reveal that amplification of undermarsh tides is lower or nonoccurring toward locations at the end of narrower side-channels (locations 2 and 3), whereas clear amplification is observed toward the end of the main channel (location 1). These variations in attenuation and amplification rates can be attributed to differences in friction, which is generally higher in narrow and shallow channels compared to wide and deep channels. Over much shorter distances, the highest attenuation rates of up to 70 cm/km are measured on the marsh platform itself (Fig. 4). This can be expected as the flow field on the marsh platform is frictionally dominated due to the high friction exerted by the vegetation present (e.g., Van Oyen et al. 2012, 2014). Taken together, our field measurements demonstrate the importance of marsh channel geometry for tidal and storm surge propagation in marshes. The results of the analytical model presented above (Fig. 7) confirm the dependency of attenuation rates of overmarsh tides on the ratio between the channel and platform width, showing clear variations in attenuation rates for different α values. Besides, these findings are in accordance with existing modeling studies, which have shown that marshes with more channels or with wider channels cause relatively lower attenuation rates compared to more continuously vegetated marsh areas (Loder et al. 2009; Temmerman et al. 2012). The

observation that attenuation rates are higher in marsh channels with a small cross-sectional area moreover indicates that marshes with a dense network of relatively narrow and shallow channels would induce higher attenuation rates than marshes with a sparser network of larger channels, although they may have a similar channel density. Unfortunately, the currently available dataset does not allow for a quantitative assessment of this hypothesis since the exact quantitative metrics of the along channel averaged channel width, channel cross-section and platform width cannot be readily evaluated for the study area with its complex branching channel network. As these data can only be retrieved by means of a specifically setup field campaign, this issue falls beyond the scope of this manuscript.

In conclusion, this field study emphasizes that flood attenuation rates in a large tidal marsh are not only location-specific, but also event-specific. An important finding of our study is that there appears to be an optimal ratio between tidal and storm surge peak water levels and marsh platform elevation which induces the strongest attenuation along the marsh channels. Hence, protection against storm surges, often attributed to coastal wetlands (e.g., Gedan et al. 2010; Shepard et al. 2011; Temmerman et al. 2013), appears to be optimal only for flood events that cause a specific range of inundation heights (0.5–1 m in this marsh) above the coastal wetland elevation. Reduced attenuation rates for higher inundation events can be caused by (1) limitations in storage area on the marsh platform during long inundation events, (2) the decreasing influence of bottom friction for higher inundation depths and (3) vegetation submergence which also reduces the friction exerted on the flow. According to our findings, high marshes would more effectively attenuate higher flood waves or severe storm surges, whereas low marshes are more effective for the attenuation of lower flood waves or regular tides. Some tidal waves might even experience amplification in higher channelized marshes due to channel convergence, especially if the marsh platform is not yet inundated. Furthermore, distinct differences in attenuation rates are observed between different sized marsh channels, while differences of up to an order of magnitude are found between marsh channels and the vegetated marsh platform, indicating the importance of marsh channel configuration and geometry for storm surge attenuation. For numerical modeling studies it is therefore essential to include the effects of channels on flood wave propagation through marshes to avoid overestimation of storm surge attenuation and correctly simulate spatial differences between surge levels. As coastal wetland conservation and restoration is starting to be implemented as part of ecosystem-based coastal defense systems our findings may help coastal managers and coastal societies with the design and morphological management of coastal wetlands to optimize their coastal defense functions.

References

Baptist, M. J., V. Babovic, J. Rodríguez Uthurburu, M. Keijzer, R. E. Uittenbogaard, A. Mynett, and A. Verwey. 2007. On inducing equations for vegetation resistance. J. Hydraul. Res. **45**: 435–450. doi:10.1080/00221686.2007.9521778

Barbier, E. B., I. Y. Georgiou, B. Enchelmeyer, and D. J. Reed. 2013. The value of wetlands in protecting Southeast Louisiana from hurricane storm surges. PLoS One **8**: e58715. doi:10.1371/journal.pone.0058715

Costanza, R., O. Pérez-Maqueo, M. L. Martinez, P. Sutton, S. J. Anderson, and K. Mulder. 2008. The value of coastal wetlands for hurricane protection. Ambio **37**: 241–248. doi:10.1579/0044-7447(2008)37[241:TVOCWF]2.0.CO;2

Friedrichs, C. T., and D. G. Aubrey. 1994. Tidal propagation in strongly convergent channels. J. Geophys. Res. **99**: 3321–3336. doi:10.1029/93JC03219

Friedrichs, C. T., and O. S. Madsen. 1992. Nonlinear diffusion of the tidal signal in frictionally dominated embayments. J. Geophys. Res. **97**: 5637–5650. doi:10.1029/92JC00354

Gedan, K. B., M. L. Kirwan, E. Wolanski, E. B. Barbier, and B. R. Silliman. 2010. The present and future role of coastal wetland vegetation in protecting shorelines: Answering recent challenges to the paradigm. Clim. Change **106**: 7–29. doi:10.1007/s10584-010-0003-7

Krauss, K. W., T. W. Doyle, T. J. Doyle, C. M. Swarzenski, A. S. From, R. H. Day, and W. H. Conner. 2009. Water level observations in mangrove swamps during two hurricanes in Florida. Wetlands **29**: 142–149. doi:10.1672/07-232.1

Loder, N. M., J. L. Irish, M. A. Cialone, and T. V. Wamsley. 2009. Sensitivity of hurricane surge to morphological parameters of coastal wetlands. Estuar. Coast. Shelf Sci. **84**: 625–636. doi:10.1016/j.ecss.2009.07.036

Lovelace, J. K. 1994. Storm-tide elevations produced by Hurricane Andrew along the Louisiana coast, August 25–27, 1992. Open File Report 94-371.

McGee, B. B. D., B. B. Goree, R. W. Tollett, B. K. Woodward, and W. H. Kress. 2006. Hurricane Rita Surge Data, Southwestern Louisiana and Southeastern Texas, September to November 2005. U.S. Geological Survey Data Series 220.

Möller, I., and others. 2014. Wave attenuation over coastal salt marshes under storm surge conditions. Nat. Geosci. **7**: 727–731. doi:10.1038/ngeo2251

Nepf, H. M. 2012. Hydrodynamics of vegetated channels. J. Hydraul. Res. **50**: 262–279. doi:10.1080/00221686.2012.696559

Nicholls, R. J., and A. Cazenave. 2010. Sea-level rise and its impact on coastal zones. Science **328**: 1517–1520. doi:10.1126/science.1185782

Resio, D. T., and J. J. Westerink. 2008. Modeling the physics of storm surges. Phys. Today **61**: 33–38. doi:10.1063/1.2982120

Shepard, C. C., C. M. Crain, and M. W. Beck. 2011. The protective role of coastal marshes: A systematic review and

meta-analysis. PLoS One **6**: e27374. doi:10.1371/journal.pone.0027374

Temmerman, S., T. J. Bouma, G. Govers, and D. Lauwaet. 2005a. Flow paths of water and sediment in a tidal marsh: Relations with marsh developmental stage and tidal inundation height. Estaries **28**: 338–352. doi:10.1007/BF02693917

Temmerman, S., T. J. Bouma, G. Govers, Z. B. Wang, M. B. De Vries, and P. M. J. Herman. 2005b. Impact of vegetation on flow routing and sedimentation patterns: Three-dimensional modeling for a tidal marsh. J. Geophys. Res. **110**: F04019. doi:10.1029/2005JF000301

Temmerman, S., M. B. De Vries, and T. J. Bouma. 2012. Coastal marsh die-off and reduced attenuation of coastal floods: A model analysis. Glob. Planet. Change **92–93**: 267–274. doi:10.1016/j.gloplacha.2012.06.001

Temmerman, S., P. Meire, T. J. Bouma, P. M. J. Herman, T. Ysebaert, and H. J. De Vriend. 2013. Ecosystem-based coastal defence in the face of global change. Nature **504**: 79–83. doi:10.1038/nature12859

Van Oyen, T., L. Carniello, A. D'Alpaos, S. Temmerman, P. Troch, and S. Lanzoni. 2014. An approximate solution to the flow field on vegetated intertidal platforms: Applicability and limitations. J. Geophys. Res. Earth Surf. **119**: 1682–1703. doi:10.1002/2013JF003064

Van Oyen, T., S. Lanzoni, A. D'Alpaos, S. Temmerman, P. Troch, and L. Carniello. 2012. A simplified model for frictionally dominated tidal flows. Geophys. Res. Lett. **39**: 1–6. doi:10.1029/2012GL051949

Van Rijn, L. C. 2011. Analytical and numerical analysis of tides and salinities in estuaries; part I: Tidal wave propagation in convergent estuaries. Ocean Dyn. **61**: 1719–1741. doi:10.1007/s10236-011-0453-0

Van der Molen, J. 1997. Tidal distortion and spatial differences in surface flooding characteristics in a salt marsh: Implications for sea-level reconstruction. Estuar. Coast. Shelf Sci. **45**: 221–233. doi:10.1006/ecss.1997.0179

Vandenbruwaene, W., C. Schwarz, T. J. Bouma, P. Meire, and S. Temmerman. 2015. Landscape-scale flow patterns over a vegetated tidal marsh and an unvegetated tidal flat: Implications for the landform properties of the intertidal floodplain. Geomorphology **231**: 40–52. doi:10.1016/j.geomorph.2014.11.020

Wamsley, T. V., M. A. Cialone, J. M. Smith, J. H. Atkinson, and J. D. Rosati. 2010. The potential of wetlands in reducing storm surge. Ocean Eng. **37**: 59–68. doi:10.1016/j.oceaneng.2009.07.018

Wamsley, T. V., M. A. Cialone, J. M. Smith, B. A. Ebersole, and A. S. Grzegorzewski. 2009. Influence of landscape restoration and degradation on storm surge and waves in Southern Louisiana. Nat. Hazards **51**: 207–224. doi:10.1007/s11069-009-9378-z

Woodruff, J. D., J. L. Irish, and S. J. Camargo. 2013. Coastal flooding by tropical cyclones and sea-level rise. Nature **504**: 44–52. doi:10.1038/nature12855

Zhang, K., H. Liu, Y. Li, H. Xu, J. Shen, J. Rhome, and T. J. Smith. 2012. The role of mangroves in attenuating storm surges. Estuar. Coast. Shelf Sci. **102–103**: 11–23. doi:10.1016/j.ecss.2012.02.021

Acknowledgments

We thank the Antwerp Port Authority for funding this research. We thank Stichting Het Zeeuwse Landschap, and especially nature guides M. Buise, W. Poppe and C. van Dueren den Hollander for their collaboration and assistance during the field work. The data presented in this article is available at the author.

Submitted 5 March 2015
Revised 10 April 2015
Accepted 13 April 2015

Associate editor: Craig Stevens